Design of an Internal Osculating Waverider Intake

Mark E. Noftz,* Andrew J. Shuck,† Joseph S. Jewell,‡ Jonathan Poggie,§
Purdue University, West Lafayette, IN, 47907, USA

Andrew N. Bustard,¶ Thomas J. Juliano‖
University of Notre Dame, Notre Dame, IN, 46556, USA

Nicholas J. Bisek**
Air Force Research Laboratory, Wright-Patterson AFB, OH, 45433, USA

The design of an inward-turning, high-speed, 3D streamline traced intake is presented from osculating axisymmetric theory. To satisfy the osculating intake design criteria, a stitched Busemann diffuser and Internal Conical Flow-A (ICFA) solution is used as the basic isentropic compressive streamline. This new contour solution, dubbed Internal Conical Flow-C (ICFC), provides efficient compression, high flow uniformity, and straight leading edge shocks of equal strength. Additionally, a novel method for constructing the lower intake capture surface is presented. The combined process leads to a new method of high-speed intake design, labeled the Osculating Internal Waverider Intake with Parallel Streamlines (OIWPS). From this method, a generic shape-transitioned intake is constructed and named the IN-Intake for the Indiana universities that contributed to the project. Computational fluid dynamic (CFD) results are assessed to validate the design method for both the 2D parent flowfields and the full 3D design. These results were contrasted against flow properties from the OIWPS code. Finally, two blockage models were designed and fabricated for blockage testing in the Boeing-AFOSR Mach 6 Quiet Tunnel.

I. Nomenclature

M = Mach Number

γ = Specific Heat Ratio

β = Oblique Shock Angle

δ = Flow Deflection Angle

*Graduate Student, School of Aeronautics and Astronautics, Student Member, AIAA, mnoftz@purdue.edu
†Graduate Student, School of Aeronautics and Astronautics, Student Member, AIAA
‡Assistant Professor, School of Aeronautics and Astronautics, Associate Fellow, AIAA
§Professor, School of Aeronautics and Astronautics, Associate Fellow, AIAA
¶Graduate Student, Department of Aerospace and Mechanical Engineering, Student Member, AIAA
‖Associate Professor, Department of Aerospace and Mechanical Engineering, Senior Member, AIAA
**Senior Research Aerospace Engineer, AFRL/RQHF, Associate Fellow, AIAA

CR = Overall Contraction Ratio

ICR = Internal Contraction Ratio

r = Radial Length Variable

θ = Angular Position Variable

u = Radial Mach Number

v = Angular Mach Number

R_o, h = Isolator Height

l = Isolator Length

AR = Geometric Aspect Ratio

n = Superellipse Factor

II. Introduction

High speed intakes have a wide variety of applications within the fields of commercial travel and space access. The purpose of an intake is to effectively capture and compress freestream air for efficient combustion. As freestream Mach number increases, mitigating stagnation pressure losses due to skin friction and shock waves become paramount design drivers. If a sufficiently large wetted area exists, then complex cooling requirements become necessary to handle the integrated heat loads. The intake should also provide undisturbed, uniform flow entering the isolator for effective combustion. Most importantly, the intake must avoid unstart, which is an aerodynamic phenomenon that drastically reduces mass capture and increases static pressure within the internal flowpath. During unstart, intake capture characteristics are dependent on the internal flow within the duct [1]. The coupled nature of the problems make intake design a challenging endeavor.

Simple two-dimensional ramp and axisymmetric intakes have been studied extensively in the open literature. Although they are easy to analyze, they lack compression efficiency and usually incorporate a high amount of on-design spillage [2]. Additionally, these intakes often feed directly into rectangular isolators, which are less structurally efficient and have higher drag and cooling requirements than round designs [3]. Therefore, for flight vehicles, it becomes desirable to create a three-dimensional intake capable of creating a uniform flow into an elliptical or circular isolator. Over the last two decades, focus has shifted to these more advanced three-dimensional designs. Analysis tools and rapid prototyping have grown in functionality and precision, giving designers more freedom to create complex geometries. Inward-turning, streamline traced intakes are usually much shorter and lighter when compared against 2D geometries for equivalent flow compression ratios. Additionally, they are more easily integrated onto vehicles because of their tailored intake shapes [4]. Other improved qualities include a decrease in overall drag, weaker cowl shocks that mitigate adverse shock-wave boundary layer interaction (SWBLI) effects, and smaller wetted areas that decrease heat loading.

However, the improvements do come with some concerns. Since contraction ratios and mass capture efficiencies are higher, the starting characteristics of the intake become problematic at off-design conditions [5]. Inward-turning designs often have to account for unfavorable starting scenarios by incorporating area relief, spill notches, and less aggressive internal contraction ratios.

The first step to designing an intake is to select a compressive parent flowfield that will capture freestream air and compress it to the desired static pressure and Mach number. One such parent flowfield is the classic Busemann diffuser, which was originally conceived of by Adolf Busemann and described by Mölder [6]. This axisymmetric flowfield is capable of very efficient compression at supersonic Mach numbers. A diagram of the Busemann flowfield is given in Figure 1. Air is captured by the intake and compressed isentropically by a conical flowfield. The intake flow then passes through an oblique shock at the throat, which reorients the flow to be parallel with the isolator. While this is a very efficient compression flowfield, its excessive overall length poses structural, drag, machinability, and heat transfer concerns [7]. Therefore, the intake must be truncated, which reduces stagnation pressure recovery. Simply truncating the intake at a certain point will result in a curved leading edge shock, which negatively impacts the downstream flow and results in a non-uniform intake exit flowfield [8]. Therefore it is desirable to have a straight leading edge shock. Mölder addressed this issue with the conical flowfield designated as internal conical flow A (ICFA) [6]. The ICFA contour can be stitched to the truncated Busemann intake to create a base flowfield, termed ICFC, that is highly efficient while retaining excellent flow uniformity.

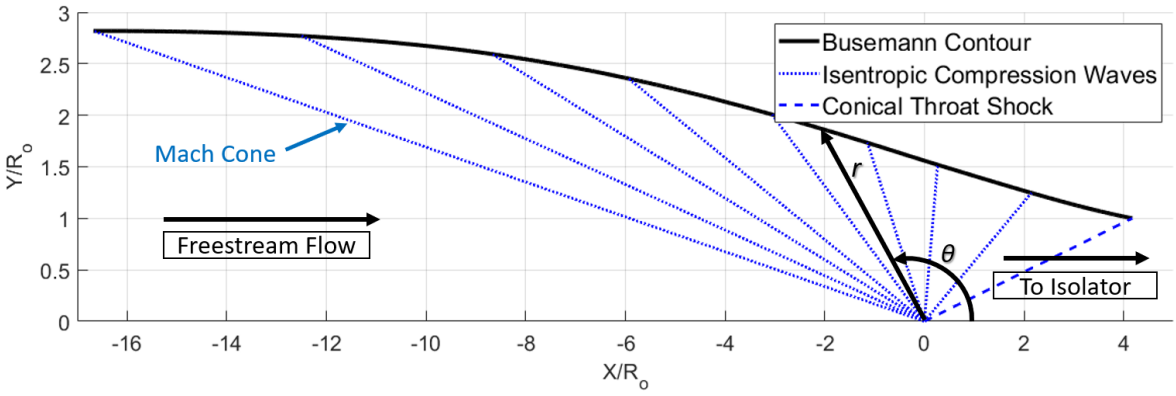

Fig. 1 Diagram of the classical Busemann flowfield described by Mölder [9]

While the ICFC is a highly efficient flowfield that is capable of satisfying all intake requirements related to preparing the flow for combustion, it fails to allow for intake start for more than very mild compression. Intake unstart can be caused by many mechanisms; large vehicle attitudes, high back pressure, and high contraction ratios in the intake are all common unstarting mechanisms [10]. For intake design, an estimate for the starting contraction limit for the overcompression mechanism is given by the Kantrowitz criterion [11]:

$$\left(\frac{A_e}{A_c}\right) = M_c \left[\frac{(\gamma+1)M_c^2}{(\gamma-1)M_c^2+2}\right]^{\frac{-\gamma}{\gamma-1}} \left[\frac{\gamma+1}{2\gamma M_c^2-(\gamma-1)}\right]^{\frac{-1}{\gamma-1}} \left[\frac{\gamma+1}{2+(\gamma-1)M_c^2}\right]^{\frac{\gamma+1}{2(\gamma-1)}} \tag{1}$$

where A_e is the exit area of the intake, A_c is the capture area of the intake, and M_c is the capture Mach number. For example, a weak throat shock in a high efficiency configuration operating at Mach 6, the Kantrowitz criterion for the minimum intake exit to capture ratio is 0.63. This, however, is considerably higher than the ratio given by the classical Busemann and ICFC style flow fields for any significant compression at high Mach numbers. Therefore, a technique has to be utilized to reduce the contraction of these highly efficient base flowfield types.

Streamtracing techniques have gained considerable attention as a method to design shape transitioned intakes. As an added benefit, streamline tracing techniques often provide ways to relieve the internal contraction ratio (ICR) of the original axisymmetric parent flowfields [3, 12]. During the design process, a capture shape and isolator exit shape are defined. If necessary, several intermediary shapes could be defined to enhance the shape transitioning process [2]. Thus, two or more streamlines from the parent flowfield are matched to follow the inner and outer radii. This creates an intake which allows for mass spillage when operating off-design and a relieved ICR that satisfies starting conditions. The blending of streamlines is a fundamentally geometric technique that is an averaged combination of several different compression streamlines. This makes the final surface definition hard to analyze analytically and necessitates CFD and experimental verification of the resulting flowfield.

The method of Osculating Axisymmetric Planes (OAP), developed by Sobieczky et al., allows designers to create complex three-dimensional wavecatcher intake geometries based on multiple two-dimensional solutions of the chosen parent flowfield [13]. This method of streamtracing follows an aerodynamic transition by solving unique parent flowfields for each defined radial slice of an intake. Historically, this method was applied to the design of high-speed waveriders [14]. Recently, however, the method of osculating planes was recently applied to the design of several three-dimensional, high-speed, and shape-transitioned intakes [15–18]. The advantages of this method include higher on-design mass capture, higher total pressure recovery, and finer control of the intake's aerodynamic properties [16]. The basic solution procedure of an OAP intake is presented in the Design Methods Section.

Viscous effects have a serious impact on the performance of a Busemann flowfield [19]. Viscous effects on shock angles, flow constriction due to boundary layer growth, and flow separation all can reduce the uniformity of intake exit flow and drastically reduce efficiency, while increasing the chances of unstart. It is therefore imperative to account for viscous effects in the design of of an intake. To offset the constriction and change in effective geometry by the presence of a boundary layer, a full viscous simulation of the intake can be run, and the geometry offset by the local displacement thickness [20]. Flow separation, which is a product of adverse pressure gradients, should be minimized as much as possible. As shock waves create large adverse pressure gradients, it is critical to investigate flow separation at walls where the shock impingement occurs. A viscous correction will be implemented in future IN-Intake studies.

III. Design Methods

A. Parent Flowfield

Constructing a high-speed intake begins with the definition of a parent flowfield. The parent flowfield chosen for the IN-Intake was an ICFC style contour, modeled after work from Zuo and Ramasubramanian [21, 22]. An ICFC parent flowfield obtains good performance by merging the ICFA solution of flow past a straight conical shock with the solution of a truncated Busemann diffuser. An example of a truncated Busemann profile is shown in Figure 2. The ICFA leading edge shock strength is a known design parameter. This combination thereby provides a modified high-speed diffuser contour that satisfies the osculating design method criterion of a straight shock wave of known strength. Calculation of both the ICFA and Busemann contours is done by solving the well-known Taylor–Maccoll equations for conical flow. A transformed set of the Taylor–Maccoll equations into Mach space was used by Mölder to describe the Busemann diffuser [9]. Equations 2 and 3 are the first-order differential equations for radial "u" and angular "v" Mach number. The streamline equation (Eq. 4) can be used to generate the outer inviscid streamline, which becomes the "wall" of the intake.

$$\frac{du}{d\theta} = v + \frac{\gamma - 1}{2} uv \frac{u + v\cot\theta}{v^2 - 1} \tag{2}$$

$$\frac{dv}{d\theta} = -u + (1 + \frac{\gamma - 1}{2} v^2) \frac{u + v\cot\theta}{v^2 - 1} \tag{3}$$

$$\frac{dr}{d\theta} = \frac{ru}{v} \tag{4}$$

Since integration of the ICFA contour ends in a singular ray, the radial, angular, and total Mach components may not necessarily match those of the Busemann contour at the merging point. Additionally, the local flow turning angle for either contour do not match at the intersection ray. Otto et al. investigated different merging procedures which attempted to rectify these differences [23]. Otto found that solving the Mach number after the local Prandtl-Meyer expansion, and then using this total Mach component as the ending point for the Busemann integration reduced downstream flow non-uniformity and shock bifurcation along the centerline axis. A merged ICFC profile is shown in Figure 3. More advanced methods involving inverse methods of characteristics and ICFC correction procedures to reduce flow expansion effects are presented by Zuo, however those methods were not pursued for the current design [24, 25]. The stitching procedure is an iterative process, and the steps are outlined below:

1) Define a leading edge deflection angle. This can be used with the freestream Mach number to calculate the leading edge oblique shock angle β using equation 5.

$$\tan\delta = 2\cot\beta \left[\frac{M_1^2 \sin^2\beta - 1}{2 + M_1(\gamma + \cos 2\beta)} \right] \tag{5}$$

2) Solve the conical flow equations (2–4) from $180 - \beta$ until a singularity angle is reached.
3) Specify the Mach number immediately ahead of the throat shock in the Busemann flowfield as well as the flow deflection angle at the throat δ. Using these quantities, calculate the intake exit Mach number and shock angle β at throat using equation 5 and the normal shock relations.
4) The starting angle for the Busemann flowfield is $\theta_{TS} = \beta - \delta$. Solve the Taylor-Maccoll ODE from this angle to the angle of the singular ICFA ray using equations 2–4.
5) There will be a mismatch between the angles at the intersection of the ICFA and Busemann contours. Using the Prandtl-Meyer expansion relations, determine whether the Mach number from the ICFA solution matches that of the Busemann contour at that point after passing through expansion waves generated by the angle mismatch.
6) Adjust the value of the throat shock angle and iterate through steps 3–5 until there is negligible difference in Mach numbers.

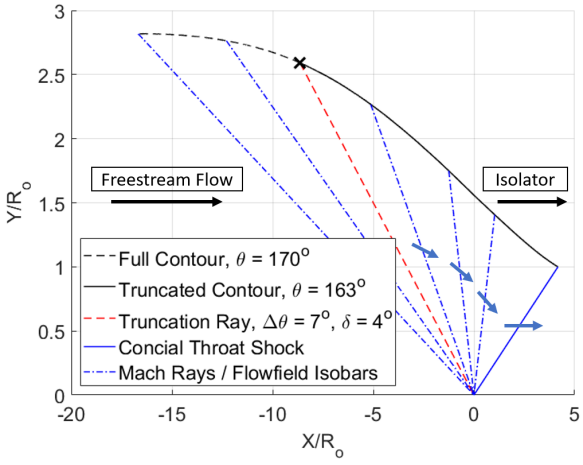

Fig. 2 Generic Truncated Busemann Contour

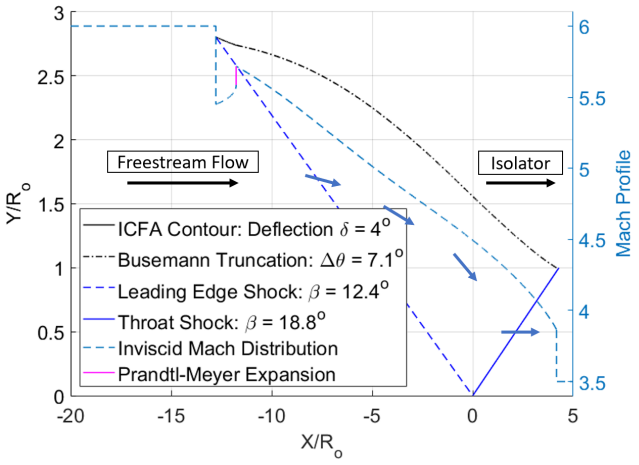

Fig. 3 Generic ICFC Contour at Mach 6

B. Osculating Design

The design of an inward-turning, shape-transitioned, high-speed intake begins with the shape definitions of the intake and isolator. The geometric superellipse family, given in parametric equations 6-8, was chosen to model these flow capture shapes due to their versatile nature. By only changing a few key parameters, a designer can quickly compare several different capture shapes that include circles, ellipses, triangles, rhombuses, rectangles, and squares. For the IN-Intake, a circular to rectangular shape transition was selected. Straight walls in the isolator section were a paramount consideration to reduce optical distortion for future experimental studies. A full list of the geometric parameters for the IN-Intake are provided in Table 1.

$$AR = \frac{l}{h} \tag{6}$$

$$x(t) = |\cos(t)|^{\frac{2}{n}} \cdot h \cdot AR \cdot sign(\cos(t)) \tag{7}$$

$$y(t) = |\sin(t)|^{\frac{2}{n}} \cdot h \cdot sign(\sin(t)) \tag{8}$$

It is common practice to define a total contraction ratio (CR) for design purposes. Although a total CR is not known until after the streamtracing process, it is still useful to define a design target. Using this approximated design CR, the streamtracing program can iterate on an isolator height that matches the target CR. During this iteration process, a static offset circle is created to check the maximum angle that an origin ray can pass through both the isolator and intake shape. A helpful visual is provided in Figure 4 to compare the intake and isolator profile. This maximum angle ray demarcates the boundary of the upper and lower surfaces for both the isolator and intake shape, respectively. Straight, fictional lines representing the intake lower surface are drawn from the max angle ray intersection to the most centered point on the isolator. This centered location represents the hypothetical cowl lip enclosure. The lower intake may deviate substantially from this representation after a full streamline tracing iteration. Thus, both internal and total contraction ratios are recalculated at the end of all completed designs.

Table 1 User Defined Geometric Inputs

Geometric Parameter	Symbol	Value
Approximated Contraction Ratio	CR_{apr}	7
Intake Aspect Ratio	AR_{in}	1
Isolator Aspect Ratio	AR_{iso}	2
Intake Superellipse Exponent	n_{in}	2
Isolator Superellipse Exponent	n_{iso}	4
Isolator Height	h	1.8
Leading Edge Deflection Angle	δ	6^o

With shapes defined, the osculating planes can be drawn from intersection rays emanating from the global origin. Rays are drawn at various azimuthal increments in the base plane, and intersection locations with the upper intake surface, upper isolator surface, and lower isolator surface are recorded. The streamtracing routine defines these as radial limits, which will be used as the limits of integration for the parent flowfields along these slices. The origin for each radial slice is then modified by the radial difference of the local lower isolator surface. Thus, a new origin or "centerbody" is defined for each unique slice, and helps to move shock intersection locations closer to the cowl lip enclosure. The max angle ray is not included as an osculating plane since there is no definable local lower isolator

surface for that slice. A view of the base shapes in the Y-Z plane is provided in Figure 5 and a completed 3D perspective of the intake with imposed oscualting planes is shown in Figure 8.

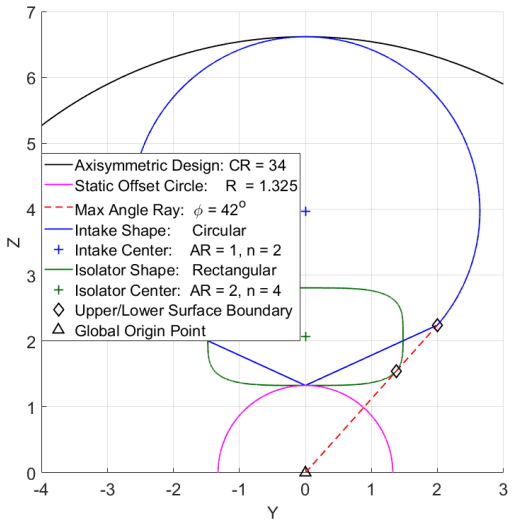

Fig. 4 Circular to Rectangular Shape Transition in the Base Plane (Unscaled Axes)

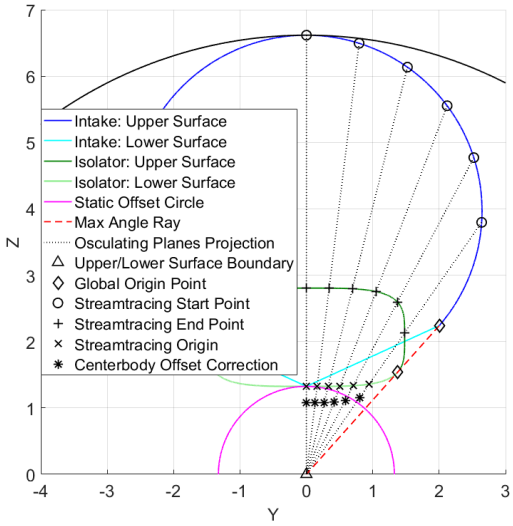

Fig. 5 Definition of Osculating Planes and the Integration Limits (Unscaled Axes)

Calculation of the parent flowfields for each osculating plane is conducted in the streamtracing program. The high-level block diagram for the code is presented in Figure 6. Integration of the Taylor-Maccoll equations is performed within the Matlab ODE-45 solver, which uses a 4th order Runge-Kutta method and a specified fixed step size. The program's inner-most loop performs the ICFA and Busemann stitching procedure. By changing the throat shock deflection angle, the Busemann contour is successively iterated until the Mach number after the Prandtl-Meyer expansion matches the Mach number of the first location on the truncated Busemann contour. Convergence is accelerated through the use of a secant method numerical solver. Imposed checks on the computed throat deflection angle ensure that the solver never exceeds the detached shock criterion for oblique shock waves.

Next, the solved "generatrix" or parent flowfield contour for a particular osculating plane is scaled appropriately by the intake's capture shape. Since the contour's exit height may not be within tolerance bounds after scaling, the pre-shock throat Mach number is iterated. This continues until a generatrix is found that matches the radial height of the isolator for that osculating plane. Shock reflection locations are solved and recorded for each slice. Since pre-shock Mach numbers and shock angles change with each osculating plane, the designer has to accept some flow distortion in the isolator. The different shock angles lead to a twisting conical shock structure, which may lead to complex conical shock wave boundary layer interaction (CSWBLI) [26]. The centerbody parameter can be iterated upon as a free variable in the streamtracing routine. This variable changes shock intersection location and thus the throat shock angle. Therefore, it allows an inverse way to tune isolator Mach number for all osculating planes. However, this option was

deactivated for the IN-Intake design to reduce geometric complexity and improve numerical convergence.

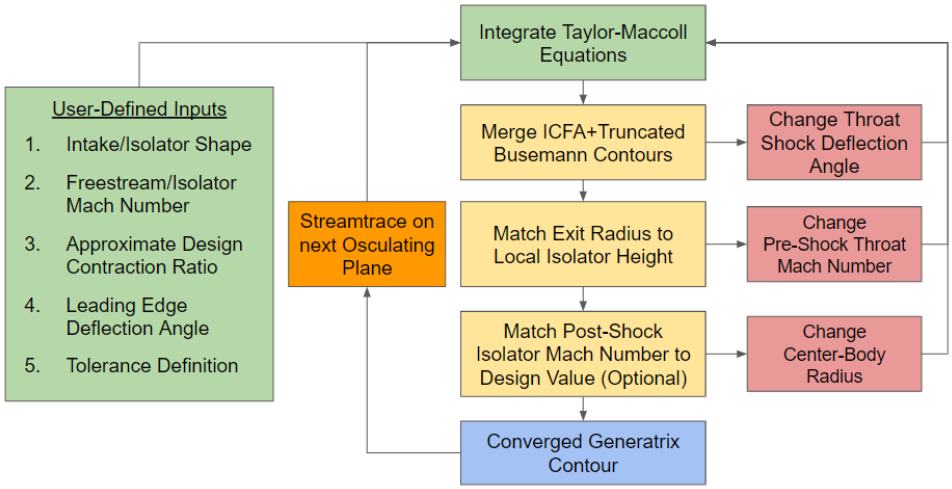

Fig. 6 Code Block Diagram of the Matlab Streamline Tracing Tool

Iteration of the pre-shock Mach number is bounded by several checks to ensure physical results. The designer is encouraged to provide good initial Mach number guesses within the bounds of the problem. A second secant method solver is used to speed convergence, and a manual step iteration method is automatically enacted if the secant solver behaves poorly. Iteration also terminates if solutions begin to consistently diverge from expected values. In the case where the loops fail to meet the tolerance criteria, the tolerances can be relaxed or better initial guesses defined based on previous solution sets. Even if an initial solution fails to converge, those final values may be replaced through a curve-fit function, saved, and interpolated for the next round of iteration.

The upper surface of the intake provides the majority of the flow compression and defines the 3D conical shock shape. In order to capture this complex shock structure for an on-design condition, the lower surface must extend forward from the isolator. Shock-on-lip condition ensures that most of the incoming mass flow successfully enters the isolator. A novel method for defining the lower surface is presented by scaling the upper generatrix surface to fit within the 3D shock structure. Thus, the lower surface of each osculating plane is defined by a scaled, parallel streamline that has the same flow turning angles as the upper surface. A completed slice of this upper and lower surface is shown in Figure 7. Validation of the combined contour and shock placement is done using 2D CFD methods described in the Computational Results Section.

The final stitching of the coupled top and bottom streamtraced surfaces occurs in unison. The contours then are simultaneously plotted for their respective osculating plane angle. A connection is drawn between the upper and lower surface contours on the maximum angle to close the intake together. A post-processing function searches for the start of the internal contraction, which begins at the forward-most point on the shortest lower surface streamline. Since the frontal capture shape is coupled to the lower surface, the total contraction ratio also needs to be re-calculated.

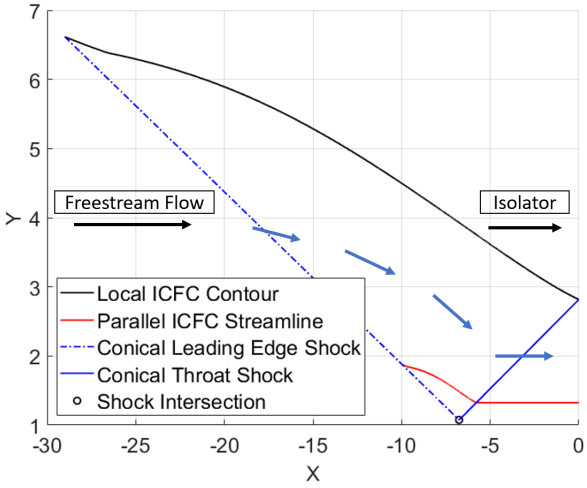

Fig. 7 Lower Surface Construction with Parallel Streamlines Methodology (Unscaled Axes)

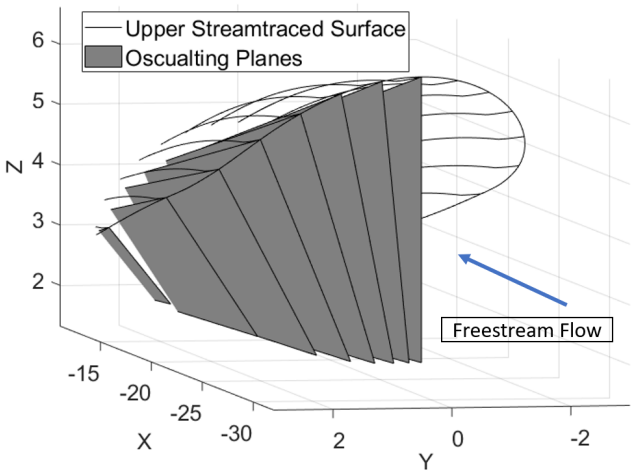

Fig. 8 Osculating Planes Overlaid with the IN-Intake (Unscaled Axes)

The contraction ratio and internal contraction ratio are 5.16 and 1.75, respectively. An isometric view presented in Figure 9 shows the frontal capture shape and outlines the start of the internal capture section. Intermediate internal profiles are also highlighted to show how the intake transitions into its final rectangular profile at the throat. The final total contraction ratio is about 26% less than the initial target. If needed, the streamtracing process can be repeated with a larger initial CR target. However, the final geometry satisfied the shape-transitioning design requirements and was pursued for testing. Lastly, this intake has a non-traditional dual cowl-notch on either side of the inward-turning compression surface. This is important because flow can spill from either notch during unstart events or off-design condition. The efficacy of this intake will be discussed in the Performance Metrics and Computational Results Sections.

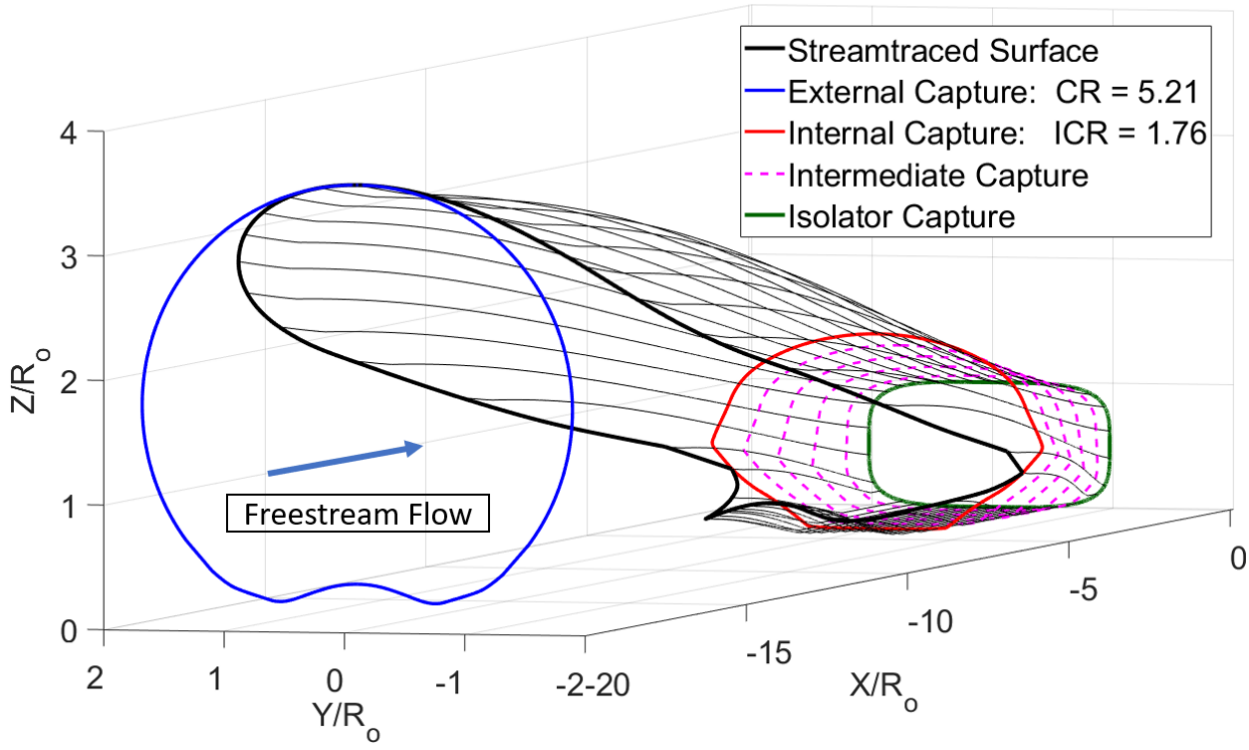

Fig. 9 Isometric View of the Completed Indiana Intake

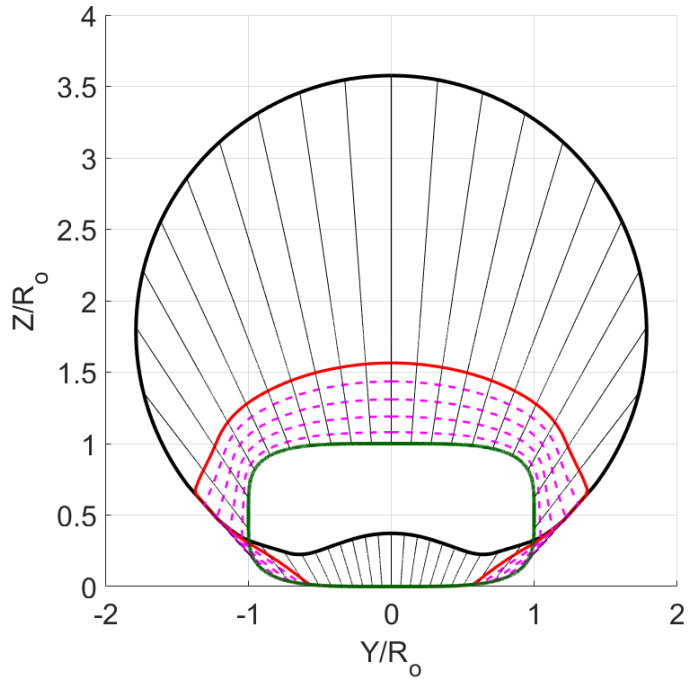

Fig. 10 Frontal Profile of the Indiana Intake

C. Performance Metrics

The IN-Intake was analyzed to determine its starting performance and other flow compression efficiency parameters. The internal contraction profile of the intake was solved by storing samples of the axial cross-sectional slices in discrete steps. These areas were then plotted over axial distance to show the gradual change in area of the internal capture section. The internal capture profile, shown in Figure 11, closely matches a linear trend. A frontal view of the intake with the internal contraction section highlighted is shown in Figure 10. It is obvious from the picture that most of the isentropic compression and flow turning occurs within the external portion of the upper-surface.

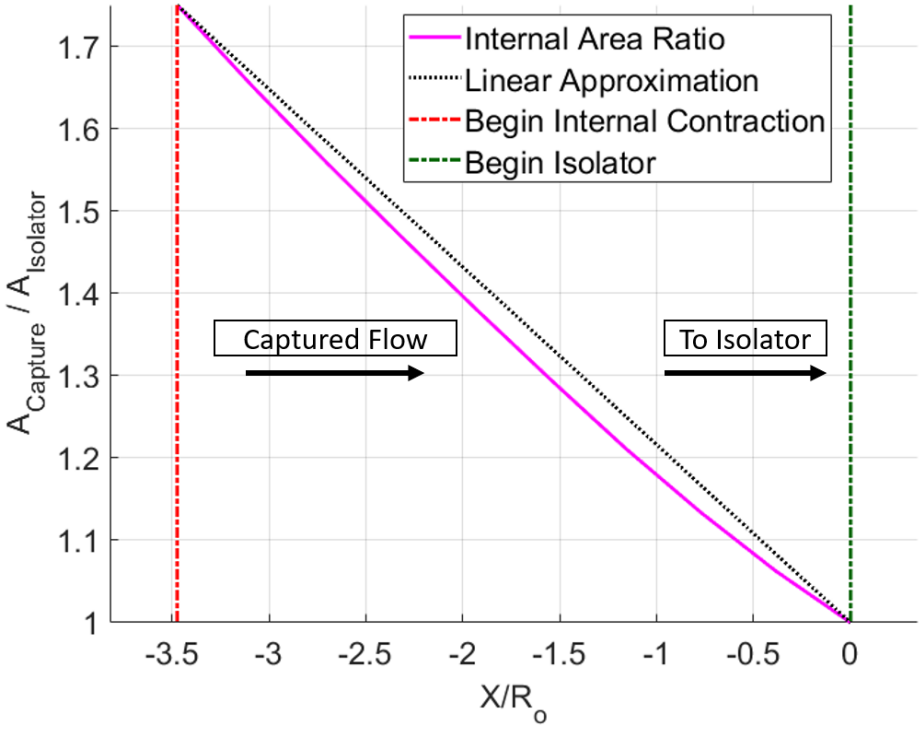

Fig. 11 Internal Area Change Profile

An established methodology for predicting an intake's startability uses the Kantrowitz criterion. As discussed in the Introduction Section, this tool helps to define intakes that will spontaneously start (above Kantrowitz Limit), operate if successfully started, or never start (below Isentropic Limit). Since the IN-Intake has an internal contraction ratio of 1.75 and a cowl closure Mach number of 4.30, it is placed within the "operable if started" category. The Kantrowitz limit is usually overly-conservative for estimating 3D inlet startability and many other correlations have been proposed to help intake designers identify more aggressive starting parameters. These limits are shown in Figure 12, and show that the IN-Intake is within the correlation limits for self-starting behavior. These experimental correlations are taken from Flock and Gülhan's review on intake starting [27]. Based on these correlations, there is high confidence that the IN-Intake will spontaneously self-start.

The streamtracing code saves all local osculating plane geometric coordinates and flow properties. Since each

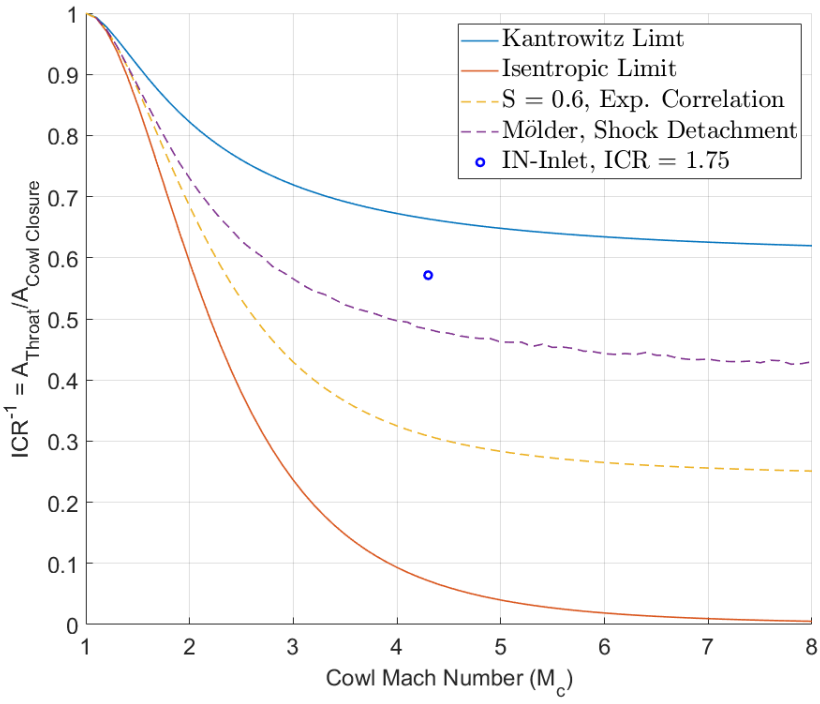

Fig. 12 Kantrowitz Plot with the IN-Intake and Predicted Cowl Mach Number

osculating plane is a unique solution to the Taylor-Maccoll equation, the starting and ending Mach numbers and pressure ratios are known from the ODE integration. The full capture area between osculating planes is known by simply projecting the shock plane to an upstream location. The areas between each osculating plane change azimuthally, so intermediate capture areas are calculable either by trapezoidal integration or Delaunay triangulation [28]. A representative plot of this technique is shown in Figure 13. Using these areas, the flow properties of the inlet can be passed into an area-weighted function for flow averaging.

The 1D area-weighted properties are useful as a baseline for future CFD and experimental comparison. A list of 1D isentropic flow properties garnered from the analytical solutions is presented in Table 2. The flow quantities can also be extracted and plotted against their respective osculating plane angle. Figure 14 shows the pre-shock and post-shock Mach numbers at the throat, along with each shock's calculated wave angle and flow deflection angle. Although the shock structure can be inferred from this graph, a better representative 3D view of the analytically defined leading edge and throat shocks can be seen in Figure 20. The analytically solved Mach distribution plots from the inviscid analysis are presented in the Computation Results section for side-by-side CFD comparison.

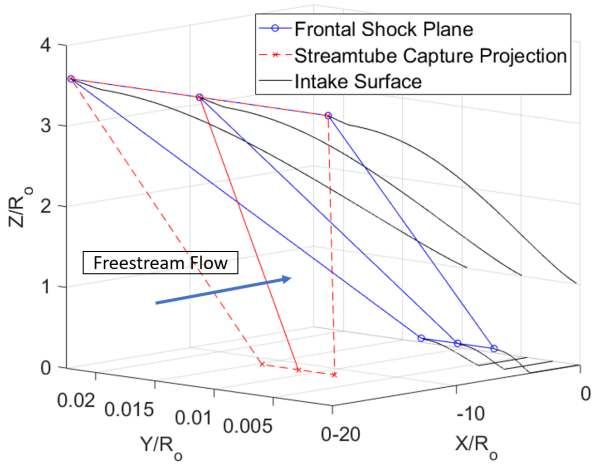

Fig. 13 Streamtube Area-Averaging Technique

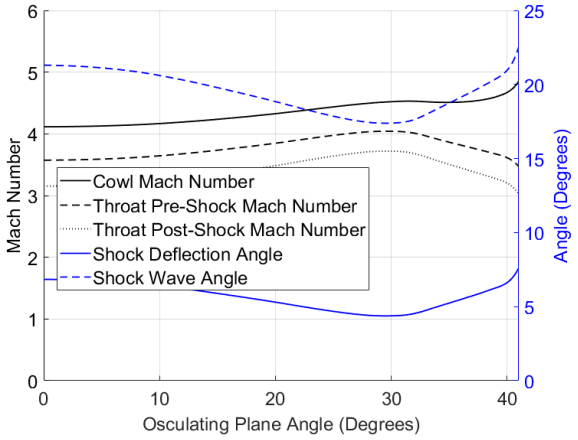

Fig. 14 Analytically Predicted Mach Numbers and Shock Angles

Table 2 1D Area-Weighted Isentropic Flow Quantities

Flow Property	Symbol	Value
Compression Ratio	P/P_∞	23.73
Total Pressure Recovery	$P_{o'}/P_o$	0.9309
Cowl Mach Number	M_c	4.30
Throat Pre-Shock Mach Number	M_2	3.76
Throat Post-Shock Mach Number	M_3	3.38

IV. Computational Results

A. Methodology

The flow conditions model the Boeing AFOSR Mach-6 Quiet Tunnel at Purdue University and are available in Table 3. This tunnel, along with the Notre Dame Large Mach-6 Quiet Tunnel, are the facilities where the intake model is being tested. The parent flowfield, lower surface streamtracing verification solutions, and a full 3D model are calculated by the CREATE-AV Kestrel code, which is an unstructured solver optimized to find solutions for various types of air vehicles. For this project, the flow is calculated with 2nd order accurate space and time methods and carried out as either inviscid or with the Spalart-Allmaras Turbulence model. The steady state solution used inviscid HLLE++ and viscous LDD+ flux schemes. More information regarding the capability and development of the CREATE-AV Kestrel code is available in Ref. [29] and [30].

Table 3 Flow Conditions

Parameter	Value
Mach	6
Freestream Velocity	873 m/s
Freestream Pressure	480 Pa
Freestream Temperature	52.8 K
Unit Reynolds Number	8.08E6 /m

1. 2D Parent Flow

The process to calculate the axisymmetric 2D parent flow starts with a Matlab generated profile which is imported into Pointwise to create a structured mesh. A grid study was conducted using 3 different resolutions: 100,000 cells (coarse), 300,000 cells (medium), and 950,000 cells (fine). The initial wall spacing were 0.008, 0.004, and 0.002 for low, medium, and high, respectively and the growth ratio was constant for each case. Solutions for each resolution were ran until they converged. This was confirmed by checking the skin friction at various iterations for each resolution. Once each resolution converged, the skin frictions were compared in Figure 15. For each mesh, there is less than a 3% max skin friction difference compared to the fine resolution. In the end, the medium resolution was used for the lower surface streamtracing calculations as a balance between fidelity and cost.

2. 3D IN-Intake

The upper and lower surface were imported into Pointwise, and a structured mesh is created. A grid study is carried out with 40 million (coarse), 120 million (medium), and 210 million (fine) cells. The initial wall spacing for each case was 0.008, 0.004, and 0.002, respectively and had a constant growth ratio between each case. Additionally, the axial spacing is clustered near the leading edge. Figure 16 shows the skin friction along the lower surface of the geometry and shows that the medium and fine grid converge with a max difference of 5% and an average of 2.6%.

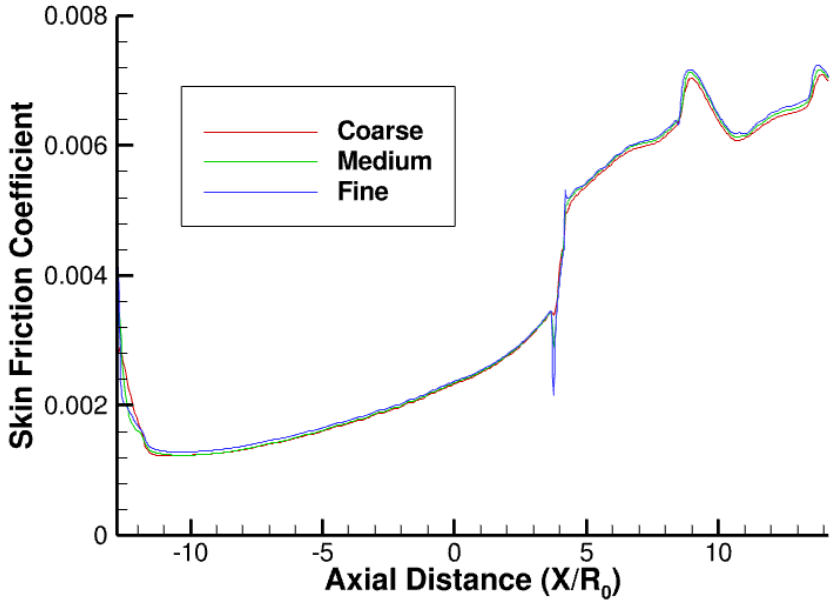

Fig. 15 Skin Friction Along the 2D ICFC Parent Surface

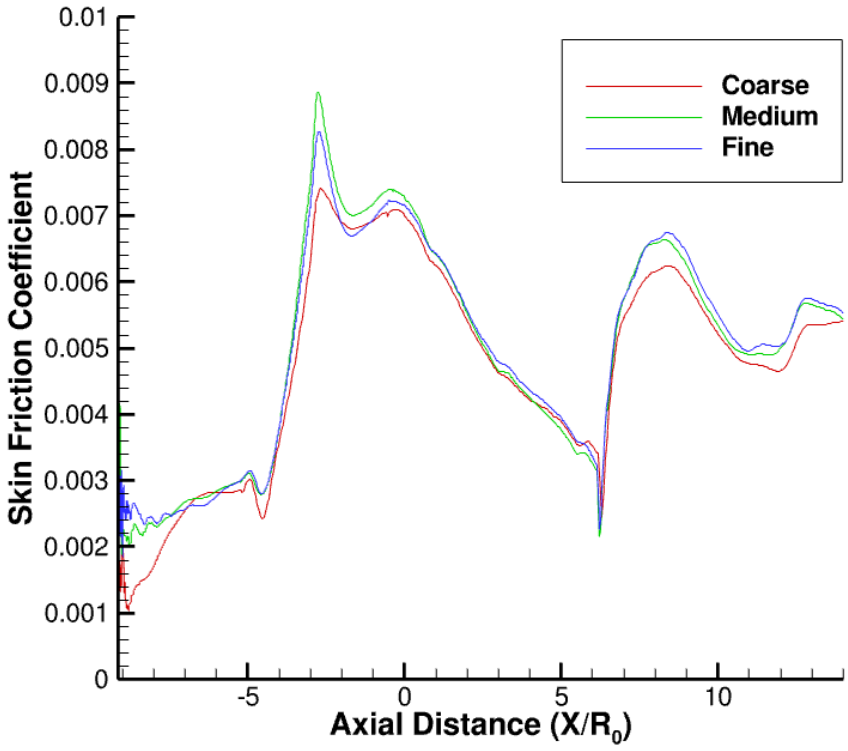

Fig. 16 Skin Friction Along the Midspan of Lower Surface of 3D IN-Intake Design

B. 2D Computational Results

1. Parent Flowfield

The 2D axisymmetric Mach contours for the sharp-inviscid, sharp-viscous, and blunt-viscous ICFC cases are presented in Figures 17a, 17b, and 17c. These solutions reveal how the ICFC flow compression process is affected by real-world viscous and blunting effects. As mentioned previously, the ICFC parent flowfield obtains good performance by merging ICFA and truncated Busemann solutions. This results in a shorter intake with good flow uniformity in the isolator. The analytical ICFC solution predicts the leading conical shock and conical throat shock to intersect at an axial distance of zero. In Figure 17a the shock structure closely matches the analytical shock intersection location, as expected. The viscous simulations shown in Figure 17b demonstrates that the presence of a boundary layer significantly affects the flow compression process the intake. The throat shock is not cancelled and significant non-uniformity is observed in the isolator. This highlights the need for a boundary layer viscous correction (BLVC) procedure for the intake surface. A BLVC is being developed for the final Indiana-Intake wind tunnel model. A blunted-viscous ICFC case was also studied. Figure 17c shows the effect of a 0.01 R/R_o blunt leading edge on the ICFC solution. Blunt leading edges cause the leading shock to intercept the centerline earlier and increases downstream Mach distortion. Overall, the influence of blunting and viscous effects work in tandem to push the shock front forward of its theoretical intersection point with the centerline.

2. Lower Surface Streamtracing Validation

A 2D slice of the combined upper-lower surface streamtracing technique with parallel streamlines (ICFC-PS) was investigated with 2D axisymmetric CFD. The Mach contour is shown in Figure 18 to evaluate the capability of the combined method. With this design, the shock passes just before the lower surface which results in a weak reflected shock. The vast majority of the flow is captured, and the throat shock impinges at the lower surface shoulder. There is excellent flow uniformity in the isolator and the lower surface streamtracing method can therefore be applied to each osculating plane to create a full 3D intake. Viscosity and bluntness effects are expected to move the shock upstream and disrupt both the downstream isentropic compression process and the shock cancellation. The final design will implement a viscous correction to minimize these effects.

C. 3D Computational Results

1. Analytical Inviscid Results

The streamlines constituting the IN-Intake were constructed from several analytical solutions to the Taylor-Maccoll equations. In addition to creating the outer wall of the intake, it is possible to extract the flow solutions and construct a first-order representation of the intake's flowfield. This analytical representation essentially stitches together all ICFC Mach distributions together for a 3D representation. The analysis method assumes that the flow is inviscid and at a

steady-state condition. Also, it does not account for bluntness effects, real gas effects, or Mach wave reflections off the bottom capture surface. The core solutions can be displayed in axial cross-sectional slices, on the intake's upper compressive surface, or along a specified osculating plane. Although the Mach number profiles are displayed here, the pressure and temperature contours can also be displayed if freestream conditions are known. For brevity, those plots were not displayed.

The Mach number profile contours reveal how the flow is compressed along each osculating plane. The surface Mach number profile, shown in Figure 19, shows the gradual compression of the flow as it progresses towards the isolator. The merging of the ICFA and truncated Busemann contours is noticeable at their stitching location. The sudden flow expansion causes a jump in surface Mach number. Additionally, shorter streamlines provide much less flow compression, as expected. This is noticeable in Figure 20, where the Mach number slices along the length of the inlet show little compression for flow at the most extreme osculating plane angles. Since the flow is still highly supersonic along these extreme rays, the shocks at the throat must be stronger to decelerate the flow. Figure 14 confirms this assumption, since there is a sharp increase in shock angle, and thus shock strength, along these outer ray angles.

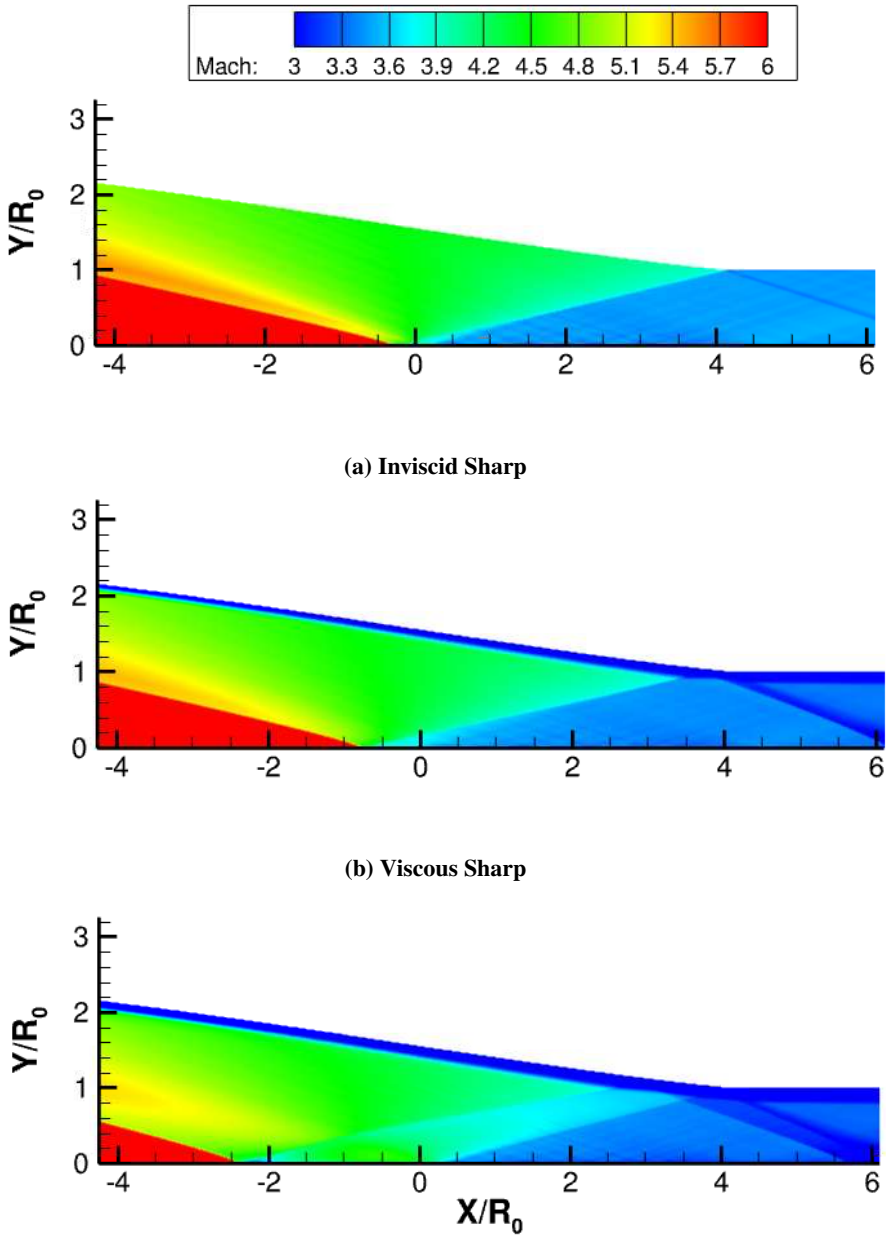

(a) Inviscid Sharp

(b) Viscous Sharp

(c) Viscous Blunt

Fig. 17 ICFC Mach Contours with: a) Inviscid Sharp, b) Viscous Sharp, and c) Viscous Blunt

2. CFD Inviscid Results

The CFD inviscid solutions deviate from the analytical results in a few key ways. For instance, in Figure 19 the Prandtl-Meyer expansion near the leading edge is not as strong as the analytical solution. For extreme osculating plane angles, the expansion region moves towards the leading edge (red-dotted circle). Also, it appears that the throat shock misses the throat shoulder, causing flow corner-turning and expansion at the throat (solid-blue double arrow). This is

caused by a shallower shock angle, which is observable in Figure 21 at the internal contraction. The analytical shock appears steeper than the invisicd CFD shock. Overall compression behavior of the inlet can be deduced from the axial Mach slices presented in Figures 20 and 21. The invisicd CFD solution shows a leading edge shock reflection off the lower surface near the start of the internal contraction. This disrupts the downstream compression process and creates downstream flow distortion. The CFD solution also shows higher Mach numbers along steep osculating plane angles near the side-cowl and lower surface. More investigation is necessary to link the loss of compression on the extreme rays to deviations from the predicted baseline performance parameters in future experiments.

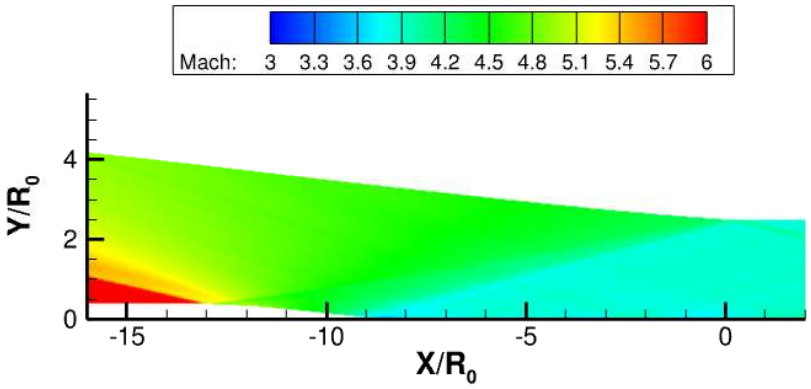

Fig. 18 ICFC-PS Inviscid Sharp Mach Contour

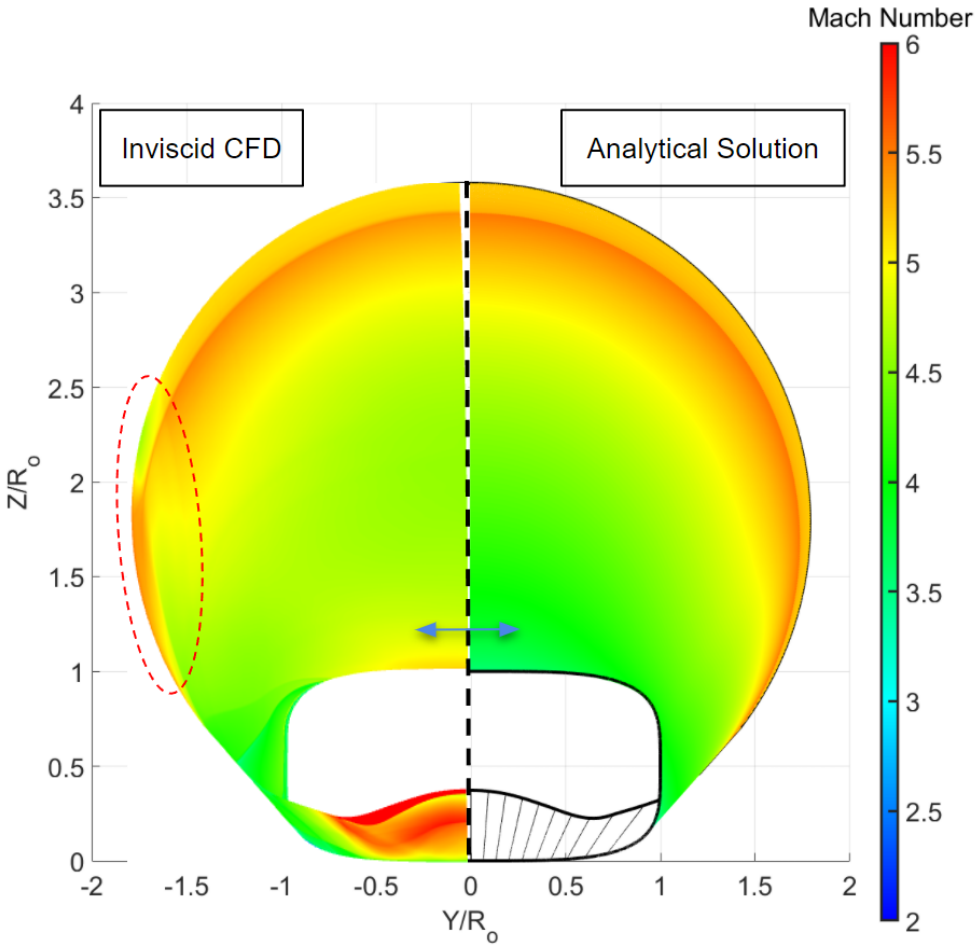

Fig. 19 Inviscid Surface Mach Contour Comparison, Frontal View

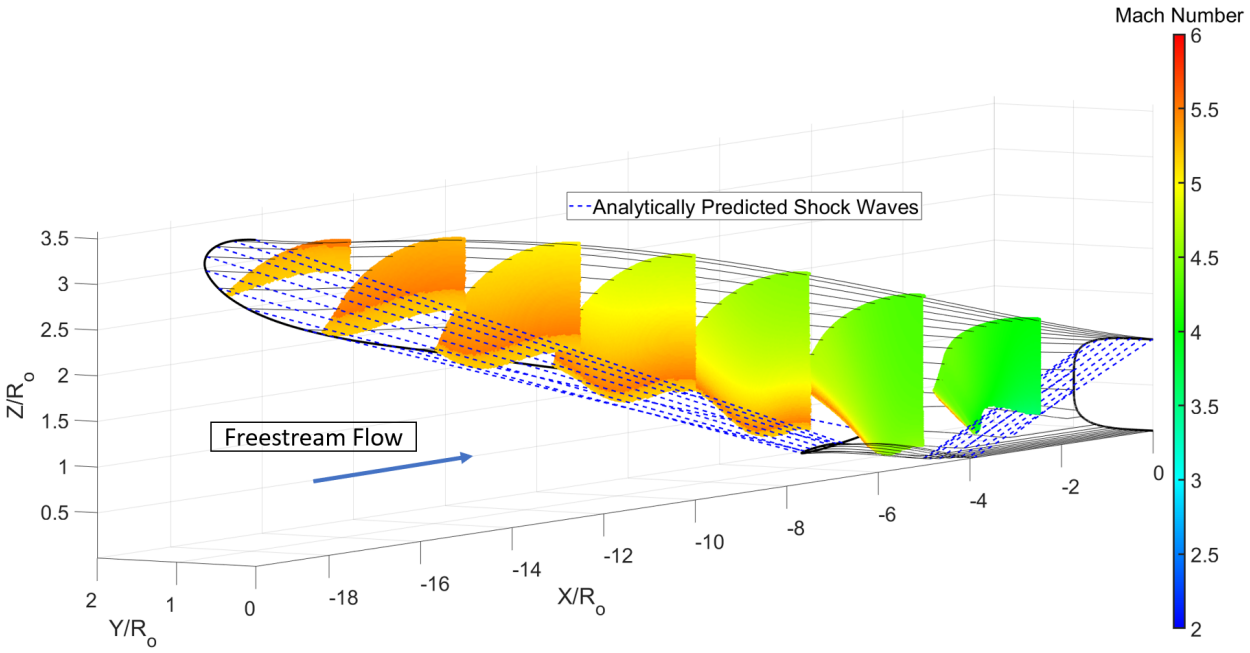

Fig. 20 Analytical Inviscid Solution: Mach Slices, $X/R_o = [2.5, 5, 7.5, 10, 12.5, 15, 17.5]$

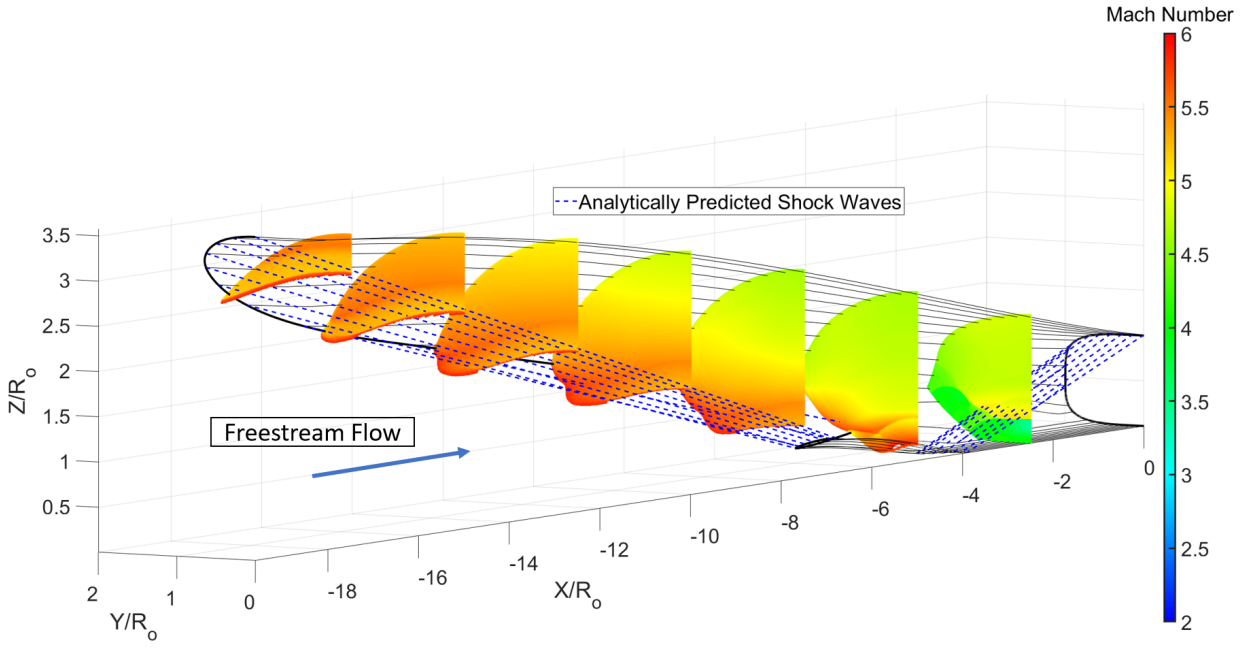

Fig. 21 CFD Inviscid Solution: Mach Slices, $X/R_o = [2.5, 5, 7.5, 10, 12.5, 15, 17.5]$

3. CFD Viscous Results

The full 3D viscous results of the IN-Intake are presented in Figures22 and 23. The conical shock emanating from the intake's lower surface is clearly visible in Figure 22, which shows axial slice pressure contours near the IN-intake throat. The conical shock reflects off the throat's upper surface and continues downstream into the isolator. The surface pressure contour of the intake and isolator are shown in Figure 23. Several regions of high pressure are seen within the isolator. These regions show where the reflected throat conical shock impinges the isolator's surface. These regions are of interest because of the likelihood of SWBLI. Additionally, a region of high pressure is seen near the cowl-lip area. This is likely due to local bow shock forming between the upper and lower surfaces. This is described in Figure 25.

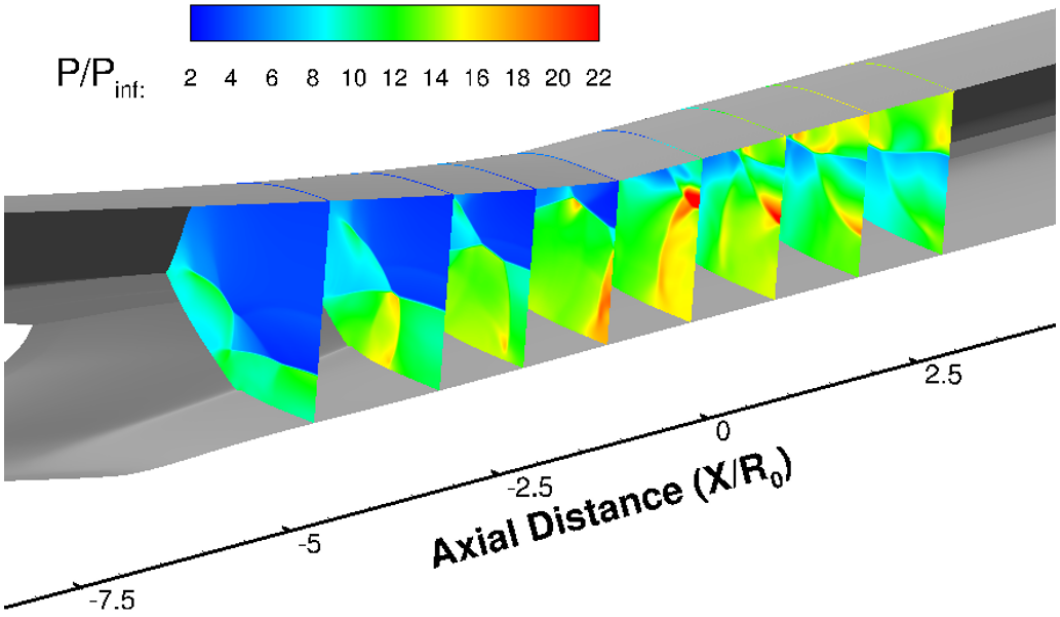

Fig. 22 Pressure Slice Contours Near IN-Intake Throat

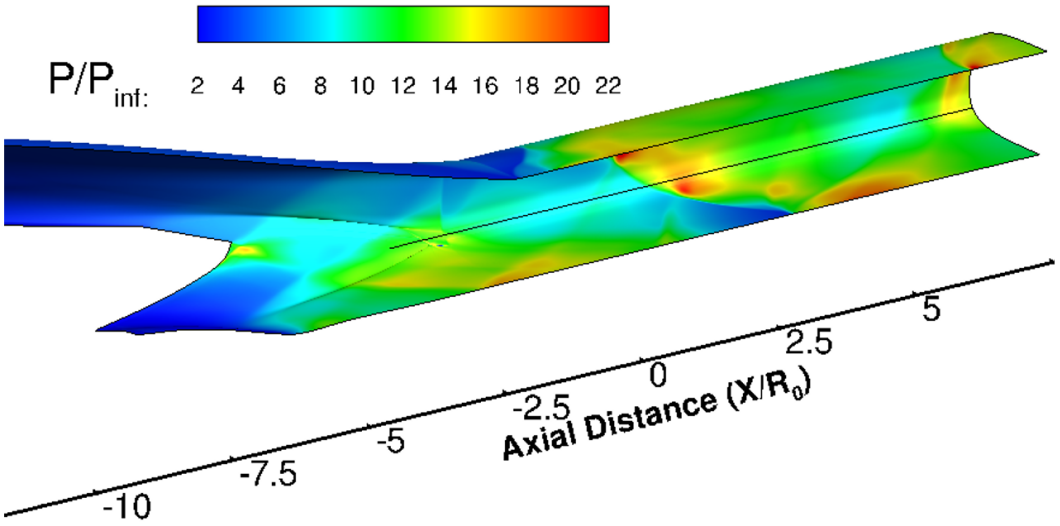

Fig. 23 Wall Pressure Contour of Intake and Isolator (Black line indicates the corner)

V. Model Generation

The analytical position vectors that define each osculating plane contain thousands of points. This level of precision was necessary to retain stability for the fixed-step numerical ODE solvers in Matlab. However, this amount of data was unnecessary and detrimental to CFD analysis and model generation. To reduce the point density, an endpoint-preserving downsampling and resampling technique was used to redefine the data set. The resampling code redefined all coordinates with respect to a reference axial distance vector that maintained a constant axial spacing. This defined spacing prevented over-fits in grid generation softwares while giving good performance for splines defined in CAD software. These data vectors were exported in i-j-k format for CFD and into csv-excel files for CAD import. Within CAD, several dozen splines were lofted together to create swept surfaces, which is pictured in Figure 24. These surfaces were then closed to create solid objects. The only non-analytical rounding required was that along the connecting surface. This area connects the top and bottom streamtraced surfaces together. Care was taken to sufficiently thicken the area to enhance strength while minimizing bluntness that can create a local bow shock, shown in Figure 25.

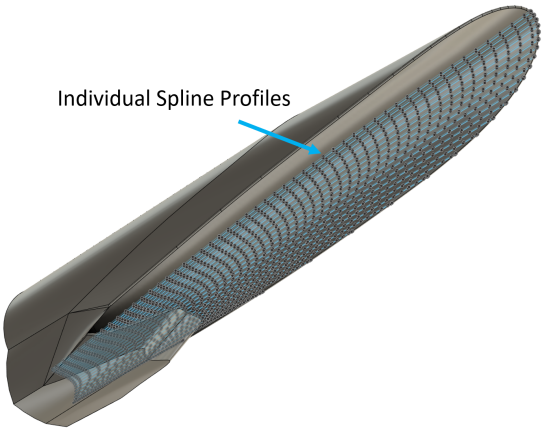

Fig. 24 IN-Intake Lofted Spline Functions for Surface Generation in CAD

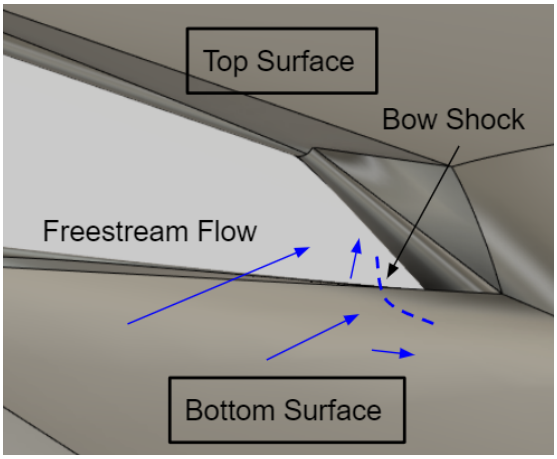

Fig. 25 IN-Intake Rounded Connecting Surface with Displaced Bow Shock

An analytical method of defining the 0.04 inch blunted leading edge was used within the streamtracing design code. A blunting method developed by O'Brien sought to preserve the original total contraction ratio of the intake [31]. This method shifted and recalculated the parent flowfield by a specified amount dictated by the leading edge radius and leading deflection angle. Additionally, the blunting edge was defined based on a tangent condition to the leading points on the contour. The stagnation streamline, which impacts the blunt leading edge, would coincide at the same location as the inviscid, sharp contour starting position and preserve contraction ratio between streamlines. Unfortunately, integrating this method into the streamtracing code was computationally expensive and complex. Additionally, for small leading edge radii, the change in total contraction ratio is minimal and negligible. A similar method was implemented that did not re-solve the parent streamline but did preserve the blunted tangency condition. This analytical technique was key to avoiding CAD complexities stemming from rounding swept leading edges. The O'Brien method is shown in Figure 26 and shows the difference in parent flowfields. In Figure 27 the highlighted splines outline the analytical definition of the blunted leading edge for osculating planes near the 0° ray. Please note how the blunt leading edge is parallel to the intake contour and not the freestream stagnation streamline.

Two IN-Intake prototype models were fabricated for a blockage study within the Boeing-AFOSR Mach 6 Quiet Tunnel (BAM6QT). A wind-tunnel blockage study was pursued to alleviate concerns regarding tunnel startability with the intakes. Wind tunnel starting is a complicated phenomenon that is not easily predicted through the use of experimental correlations or CFD. Although frontal area plays a significant role in determining total blockage, other factors like model pitch, non-conformal windows, boundary layer separation, boundary layer thickness, and SWBLI all play a role in determining tunnel startability [32]. A blockage plot based on 1D normal shock theory is presented in Figure 28 to show a sample legacy method at predicting tunnel starting. A list of other models that have been successfully tested in the Boeing-AFOSR Mach 6 quiet tunnel are also shown with the exception of the 14% HIFiRE-6

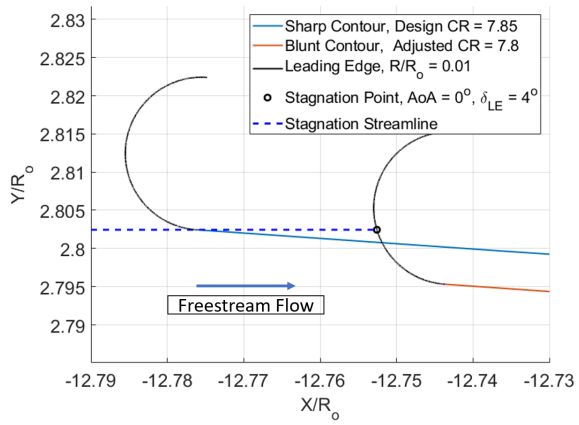

Fig. 26 O'Brien Construction Method for an Intake's Blunt Leading Edge

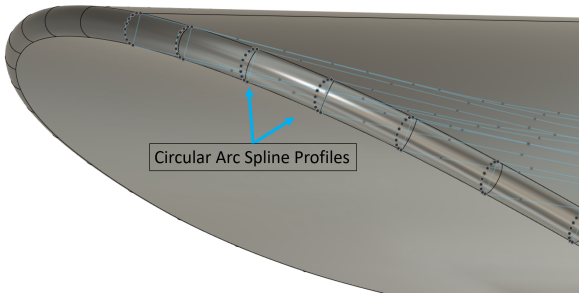

Fig. 27 Blunted Spline Profile for Leading Edge Generation in CAD

model. However, many of these are axisymmetric slender models with sharp leading edges. The intake models are neither axisymmetric nor slender. Additionally, they contain inner flow paths that may interact to unstart the tunnel. The two blockage models are similar in frontal area due to the smaller inlet requiring larger wall thicknesses to retain structural rigidity in the tunnel. However, the lengths of the models are drastically different and presented in Table 4 for comparison.

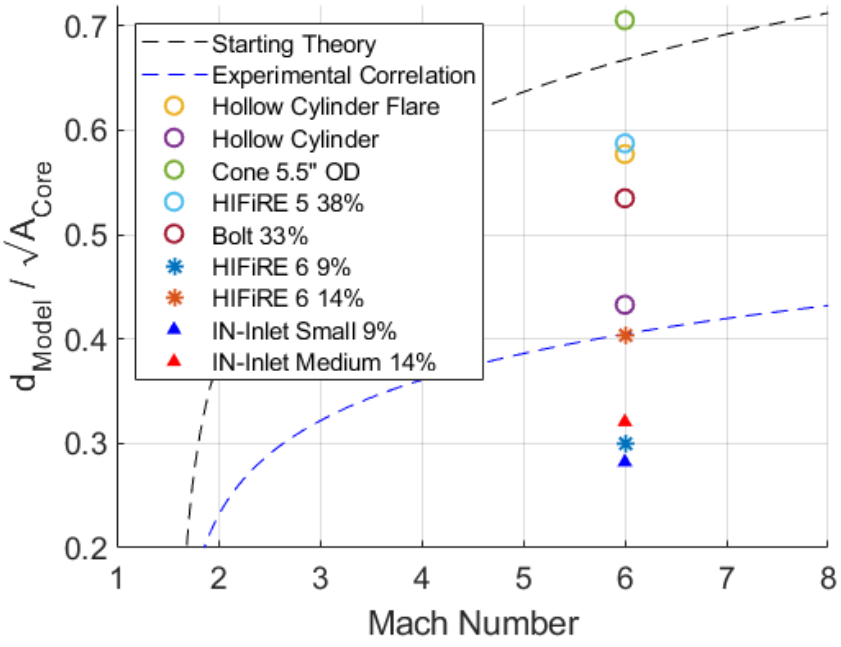

Fig. 28 Wind Tunnel Starting Correlation with Viscous-Corrected Core Flow, Reproduced from Pope [32]

The smallest IN-Intake model was scaled similarly to the 9% HIFiRE-6 202E model. This HiFIRE-6 model, on loan from the Air Force Research Laboratory, had previously undergone testing within the BAM6QT. Results showed

Table 4 IN-Intake Model Parameters

	Small	Medium
Scale (%)	9	14
Throat Height R_0 (in.)	0.34	0.53
Throat Width (in.)	0.68	1.06
Corrected Throat Height (in.)	0.44	0.73
Intake X/R_0	19.5	19.5
Intake Length (in.)	6.66	10.34
Isolator X/R_0	15	15
Isolator Length (in.)	5.10	7.95
Nozzle X/R_0	5	5
Nozzle Length (in.)	1.70	2.65
Total Length (in.)	13.46	20.94

that the BAM6QT successfully started with the model pitched at a variety of angles of attack and different freestream Reynolds numbers. A larger IN-Intake version, dubbed "Medium Intake", was scaled to a 14% HIFiRE-6 202E size and used to test the limits of tunnel starting. These blockage models were based on an early version of the streamtracing design code. Due to a change in the program, these preliminary models have an over-sized lower lip surface, so pressure measurements and performance may deviate from the finalized model due to changes in geometry and shock structure. A table of the IN-Intake blockage model design dimensions are shown in Table 4.

The IN-Intake blockage test campaign was conducted inside the Boeing-AFOSR Mach 6 Quiet Tunnel (BAM6QT) at Purdue University. Wind tunnel startability was measured over a range of freestream unit Reynolds numbers for both scaled models. Analysis of the experimental results will be discussed in future publications. Additionally, an in-depth analysis of the intake's started and unstarted states will be presented from time-dynamic IML static pressure measurements.

VI. Conclusion

A discussion of high speed intake requirements and design methods has been presented. An analytical code for an osculating intake design based on a parent ICFC-PS flowfield has been written. Results from the Matlab code are presented for both the parent flowfield and a streamline traced intake design. Two-dimensional CFD was conducted for analytical code verification and to validate the lower surface streamtracing technique. An intake geometry suitable for testing in the Boeing AFOSR Mach-6 Quiet Tunnel at Purdue University and the AFOSR Notre Dame Large Mach-6 Quiet Tunnel at the University of Notre Dame has been generated for an on-design condition of Mach 6. Three-dimensional CFD of the intake has been presented and compared to the OIWPS design's expected performance estimates. Finally, full mechanical design was conducted and two blockage models were created for testing. The starting envelope of the Inidiana-Intake and the BAM6QT tunnel were quantified from known correlations. A future paper will

discuss results from the blockage test campaign for both the small and medium intakes conducted within the BAM6QT.

Acknowledgments

This work was supported by the U.S. Air Force Research Laboratory under Award Number FA8650-20-2-240 and cleared for pubic release under Case Number AFRL-2021-3864. Computational resources were provided by the Air Force Research Laboratory DoD Supercomputing Resource Center and the Engineer Research and Development Center DoD Supercomputing Resource Center. The authors are indebted to S. Cox-Stouffer and R. Baurle for guidance related to the literature on inlet design.

References

[1] Heiser, W. H., and Pratt, D. T., *Hypersonic Airbreathing Propulsion*, AIAA, 1994, pp. 197–266. Education Series.

[2] Smart, M. K., "Design of Three-Dimensional Hypersonic Inlets with Rectangular-to-Elliptical Shape Transition," *Journal of Propulsion and Power*, Vol. 15, No. 3, 1999, pp. 408–416. https://doi.org/10.2514/2.5459.

[3] Smart, M., and Ruf, E., "Free-Jet Testing of a REST Scramjet at Off-Design Conditions," AIAA Paper 2006-2955, American Institute of Aeronautics and Astronautics, 2006, p. 1–12. https://doi.org/10.2514/6.2006-2955.

[4] Bulman, M., and Siebenhaar, A., "The Rebirth of Round Hypersonic Propulsion," AIAA Paper 2006-5035, American Institute of Aeronautics and Astronautics, 2006, pp. 1–8. https://doi.org/10.2514/6.2006-5035.

[5] You, Y., "An Overview of the Advantages and Concerns of Hypersonic Inward Turning Inlets," 2011. https://doi.org/10.2514/6.2011-2269.

[6] Mölder, S., "Internal, axisymmetric, conical flow." *AIAA Journal*, Vol. 5, No. 7, 1967, pp. 1252–1255. https://doi.org/10.2514/3.4179.

[7] Ogawa, H., Mölder, S., and Boyce, R., "Effects of Leading-Edge Truncation and Stunting on Drag and Efficiency of Busemann Intakes for Axisymmetric Scramjet Engines," *Journal of Fluid Science and Technology*, Vol. 8, No. 2, 2013, pp. 186–199. https://doi.org/10.1299/jfst.8.186.

[8] O'brien, T. F., and Colville, J. R., "Analytical Computation of Leading-Edge Truncation Effects on Inviscid Busemann-Inlet Performance," *Journal of Propulsion and Power*, Vol. 24, No. 4, 2008, pp. 655–661. https://doi.org/10.2514/1.30178.

[9] Mölder, S., and Timofeev, E., "Hypersonic Air Intake Design for High Performance and Starting," *RTO-EN-AVT-195*, 2019, pp. 1–40.

[10] Chang, J., Li, N., Xu, K., Bao, W., and Yu, D., "Recent research progress on unstart mechanism, detection and control of hypersonic inlet," *Progress in Aerospace Sciences*, Vol. 89, 2017, pp. 1–22. https://doi.org/https://doi.org/10.1016/j.paerosci.2016.12.001.

[11] Kantrowitz, A., and Donaldson, C., "Preliminary Investigation of Supersonic Diffusers," *NACA Wartime Report*, Vol. ACR-L5D20, 1945, pp. 1–25.

[12] Billig, F., Baurle, R., Tam, C.-J., and Wornom, S., "Design and analysis of streamline traced hypersonic inlets," *9th International Space Planes and Hypersonic Systems and Technologies Conference*, 1999. https://doi.org/10.2514/6.1999-4974.

[13] Sobieczky, H., Dougherty, F., and Jones, K., "Hypersonic Waverider Design from Given Shock Waves," *Proc. First International Waverider Symposium, University of Maryland*, 1990, pp. 1–20.

[14] Jones, K., and Center, K., "Waverider Design Methods for Non-Conical Shock Geometries," AIAA Paper 2002-3204, American Institute of Aeronautics and Astronautics, 2002, pp. 1–14. https://doi.org/10.2514/6.2002-3204.

[15] You, Y., Liang, D., and Cai, K., "Numerical Research of Three-Dimensional Section Controllable Internal Waverider Hypersonic Inlet," AIAA Paper 2008-4708, American Institute of Aeronautics and Astronautics, 2008. https://doi.org/10.2514/6.2008-4708.

[16] You, Y., and Liang, D., "Design concept of three-dimensional section controllable internal waverider hypersonic inlet," *Science in China Series E: Technological Sciences*, Vol. 52, No. 7, 2009, pp. 2017–2028. https://doi.org/10.1007/s11431-009-0125-1.

[17] Xuzhao, H., Jialing, L., Zheng, Z., Penfei, M., and Yingchuan, W., "Osculating Inward turning Cone Waverider/Inlet (OICWI) Design Methods and Experimental Study," AIAA Paper 2012 5810, American Institute of Aeronautics and Astronautics, 2012. https://doi.org/10.2514/6.2012-5810.

[18] Hang, Z., and Zhiguang, J., "A novel approach for inverse design of three-dimensional shock waves under non-uniform flows," *Acta Astronautica*, Vol. 176, 2020, pp. 324–331. https://doi.org/10.1016/j.actaastro.2020.06.050.

[19] Flock, A. K., and Gülhan, A., "Viscous Effects and Truncation Effects in Axisymmetric Busemann Scramjet Intakes," *AIAA Journal*, Vol. 54, No. 6, 2016, pp. 1881–1891. https://doi.org/10.2514/1.J054287.

[20] Walsh, P., Tahir, R., and Molder, S., "Boundary-layer Correction for the Busemann Hypersonic Air Inlet," *Canadian Aeronautics and Space Journal*, Vol. 49, 2003, pp. 11–17. https://doi.org/10.5589/q03-003.

[21] Fengyuan, Z., and Huang, G., "A Preliminary Overview analysis on the Internal Waverider Inlets for Ramjet," AIAA Paper 2017-2420, American Institute of Aeronautics and Astronautics, 2017. https://doi.org/10.2514/6.2017-2420.

[22] Ramasubramanian, V., Lewis, M., and Starkey, R., "Performance of Various Truncation Strategies Employed on Hypersonic Busemann Inlets," AIAA Paper 2009-7249, American Institute of Aeronautics and Astronautics, 2009. https://doi.org/10.2514/6.2009-7249.

[23] Otto, S. E., Trefny, C. J., and Slater, J. W., "Inward-Turning Streamline-Traced Inlet Design Method for Low-Boom, Low-Drag Applications," *Journal of Propulsion and Power*, Vol. 32, No. 5, 2016, pp. 1178–1189. https://doi.org/10.2514/1.B36028.

[24] Fengyuan, Z., Huang, G., Huihui, H., and Xia, C., "Analyzing the flow pattern of inward turning inlet combined with variable-geometry," AIAA Paper 2016-4574, American Institute of Aeronautics and Astronautics, 2016. https://doi.org/10.2514/6.2016-4574.

[25] Zuo, F., Huang, G., and Xia, C., "Investigation of internal-waverider-inlet flow pattern integrated with variable-geometry for TBCC," *Aerospace Science and Technology*, Vol. 59, 2016, pp. 69–77. https://doi.org/https://doi.org/10.1016/j.ast.2016.10.009.

[26] Zuo, F.-Y., and Mölder, S., "Hypersonic wavecatcher intakes and variable-geometry turbine based combined cycle engines," *Progress in Aerospace Sciences*, Vol. 106, 2019, pp. 108–144. https://doi.org/https://doi.org/10.1016/j.paerosci.2019.03.001.

[27] Flock, A. K., and Gülhan, A., "Modified Kantrowitz Starting Criteria for Mixed Compression Supersonic Intakes," *AIAA Journal*, Vol. 57, No. 5, 2019, pp. 2011–2016. https://doi.org/10.2514/1.J057283.

[28] MATLAB, *Working with Delaunay Triangulations*, The MathWorks Inc., Natick, Massachusetts, 2021.

[29] McDaniel, D. R., and Tuckey, T., "HPCMP CREATE^{TM}-AV Kestrel New and Emerging Capabilities," 2020-1525, American Institute of Aeronautics and Astronautics, 2020. https://doi.org/10.2514/6.2020-1525.

[30] Morton, S. A., and McDaniel, D. R., "HPCMP CREATE^{TM}-AV Kestrel Architecture Capability and Future Direction," 2018-0025, American Institute of Aeronautics and Astronautics, 2018. https://doi.org/10.2514/6.2018-0025.

[31] O'Brien, T., and Colville, J., "Blunt Leading Edge Effects on Inviscid Truncated Busemann Inlet Performance," AIAA Paper 2007-5411, American Institute for Aeronautics and Astronautics, 2007. https://doi.org/10.2514/6.2007-5411.

[32] Pope, A., and Goin, K. L., *High-speed wind tunnel testing*, Wiley, New York, 1965.